Journal of Nuclear Materials 494 (2017) 227–239

Contents lists available at ScienceDirect

Journal of Nuclear Materials

journal homepage: www.elsevier.com/locate/jnucmat

Scanning electron microscopy examination of a Fast Flux Test Facility irradiated U-10Zr fuel cross section clad with HT-9

Jason M. Harp*, Douglas L. Porter, Brandon D. Miller, Tammy L. Trowbridge, William J. Carmack

Idaho National Laboratory, Characterization and Advanced PIE Division, P.O. Box 1625, Idaho Falls, ID 83415, USA

HIGHLIGHTS

- Observations from a scanning electron microscopy examination of irradiated U-10Zr fuel are presented.
- The redistribution of Zr in irradiated U-10Zr fuel at this local condition was evaluated.
- The microstructure present in fuel cladding chemical interaction (FCCI) layers included some previously unobserved behavior.

ARTICLE INFO

Article history:
Received 2 May 2017
Received in revised form
3 July 2017
Accepted 21 July 2017
Available online 22 July 2017

Keywords:
Irradiated fuel
Scanning electron microscopy
U-10Zr
Fuel cladding chemical interaction (FCCI)
Zirconium redistribution

ABSTRACT

Observations from a scanning electron microscopy examination of irradiated U-10Zr fuel are presented. The sample studied had a local burnup of 5.7 atom percent and a local inner cladding temperature of 615 °C. This examination by electron microscopy has concentrated on producing data relevant to facilitating a better understanding of Zr redistribution in irradiated U-10Zr fuel and on a better understanding of the complex microstructure present in fuel cladding chemical interaction (FCCI) layers. The presented zirconium redistribution data supplements the existing literature by providing a data set at these particular local conditions. In addition to FCCI layers that are readily visible in optical microscopy, this examination has revealed lanthanide degradation of the cladding by what appears to be a grain boundary facilitated pathway. Precipitates of fission produced Pd-lanthanide compounds were observed in the fuel. Precipitated regions with elevated Mo and elevated W content were also observed in the HT-9 cladding of this sample.

© 2017 Elsevier B.V. All rights reserved.

1. Introduction

The performance of metallic fuel in a fast reactor can depend on several factors including fuel alloy, swelling (smeared density), fuel constituent redistribution, and fuel/cladding chemical interaction (FCCI) [1]. The Mechanistic Fuel Failure (MFF) series of metallic fuel irradiations were performed at the Fast Flux Test Facility (FFTF) as part of fuel qualification of metal-fueled driver fuel assemblies for the conversion of FFTF from oxide to metallic fuel [2]. These irradiations tested fuel performance of metallic fuel at a wide range of conditions including high temperature and high burnup. Several pins from MFF3 and MFF5, which operated at the highest cladding temperatures of the MFF series, were examined previously and the performance of these assemblies were evaluated using conventional postirradiation examination (PIE) techniques at the Idaho National Laboratory (INL) Hot Fuel Examination Facility (HFEF) [3,4]. While these examinations provide a wealth of performance data, a greater phenomenological understanding of FCCI and fuel constituent redistribution can be achieved utilizing more advanced techniques including electron microscopy of various forms. Microstructural characterization of irradiated fuel by electron microscopy has often been limited to small samples [5–7] or to specialized hot-cell modified devices [8]. With over 20 years since the end of irradiation of the MFF pins, it is possible to now examine some full fuel pin cross sections in non-shielded facilities such as the INL Electron Microscopy Laboratory (EML).

In this work, a cross section from an MFF3 pin (#193045), taken at an axial location near the top of the fuel column length (X/L = 0.98), was examined by scanning electron microscopy (SEM). This cross section is the same sample examined by optical

* Corresponding author.
E-mail address: jason.harp@inl.gov (J.M. Harp).

http://dx.doi.org/10.1016/j.jnucmat.2017.07.040
0022-3115/© 2017 Elsevier B.V. All rights reserved.

microscopy in Ref. [3]. A full explanation of the as-built condition and irradiation conditions of the fuel can be found in Ref. [4]. In summary, the fabricated fuel was U with 10 wt percent Zr. The fuel slugs were cast into quartz molds to achieve to 75% smeared density in relation to the cladding inner diameter and sodium bonded to the HT-9 cladding (a ferritic martensitic steel developed for fast reactor applications). The SEM examination focused on evaluating the phenomenon of radial constituent redistribution in an effort to generate more contemporary data that is comparable to similar radial redistribution data generated by EPMA presented in Refs. [9] and [10] on pins from EBR-II experimental assemblies X447 and X419. The second focus of the SEM examinations was the exploration of the fuel layers related FCCI. This cross section allows for the examination of areas where FCCI was formed and areas where it was not formed in the same sample. This current study has shown that using these aged samples and state-of-the-art equipment allow FCCI layers observed in this work appear to be more complex than those reported in Refs. [8,11,12] for similar fuel. In the FCCI layers, the observation of lanthanide elements infiltrating along prior austenite grain boundaries and this potential impact on cladding integrity highlight the importance of moving beyond optical microscopy examinations when evaluating fuel performance at design margin and near design margin conditions. Additional precipitates and microstructural features related to different regions of the fuel and cladding in the examined cross section will also be discussed.

2. Experiment

The fuel slugs for MFF pins were generated by counter gravity vacuum casting into quartz molds at Argonne National Laboratory - West. Each pin contained 2 or 3 fuel slugs with 75% smeared density compared to the cladding inner diameter. The fuel slug diameter was 0.498 cm. The slugs were sodium bonded to the cladding to ensure good thermal conductance prior to fuel swelling. The cladding was 0.686 cm outer diameter and 0.574 cm inner diameter HT-9 tubing. The HT-9 cladding has a nominal composition of Fe-12Cr-0.2C-0.25Si-0.2Mn-0.5W-0.5 V-1Mo-0.5Ni where the number preceding the element is the weight percent and Fe is the balance of the composition [13]. The ferritic martensitic alloy HT-9 was chosen for cladding due to its superior resistance to swelling and history of successful irradiation use in EBR-II [2]. The MFF-3 assembly was irradiated for 9 cycles in FFTF (from November 1988 to March 1992) to an average burnup of 10.85 atom % and a peak burnup of 13.8 atom %. The MFF-3 pin 193045, studied in this work, had a peak burnup of 12.4 atom % and was 5.7 atom% locally in the sample studied from X/L = 0.98. The time averaged irradiation temperature of the inner cladding surface for the sample at X/L = 0.98 was 615 °C. Additional information in the irradiation history can be found in Reference [3]. After irradiation in FFTF, the MFF fuel assemblies were returned to INL and stored in HFEF until PIE was initiated in 2013 [4]. Baseline PIE included neutron radiography, evaluation of axial fission product redistribution by gamma spectrometry, dimensional inspection, fission gas release and assay analysis of the gas, optical microscopy of fuel cross sections at several heights, microhardness testing of the cladding and fuel-cladding interaction zones, and chemical isotopic analysis for burnup. The results of these exams are detailed in Refs. [3,4].

Of the five samples taken from MFF3 Pin 193045, three samples exhibited FCCI in optical metallography exams. Of these three the sample from X/L = 0.98 had the lowest local burnup and consequently the lowest dose rate of these samples. This dose rate was adequately low enough to allow for hands-on loading into electron microscopy instruments. The cross section from X/L = 0.98 was mounted in a 3.2 cm steel ring designated MNT-83T. This sample is the primary subject of this work. Prior to SEM examination the cross section was re-polished to remove layers of oxide that had built up on the sample surface. The region of highest oxidation is still visible in the examination results. This region corresponds to the region of the fuel with the lowest Zr content. Oxidation even in low O_2 partial pressure environments is often problematic with U-Zr alloys and the oxidation rate increases as the Zr content is lowered. After initial re-polishing at HFEF the sample was transferred to the EML glovebox where additional hand polishing with 1 μm diamond suspension was used to remove a small oxidation

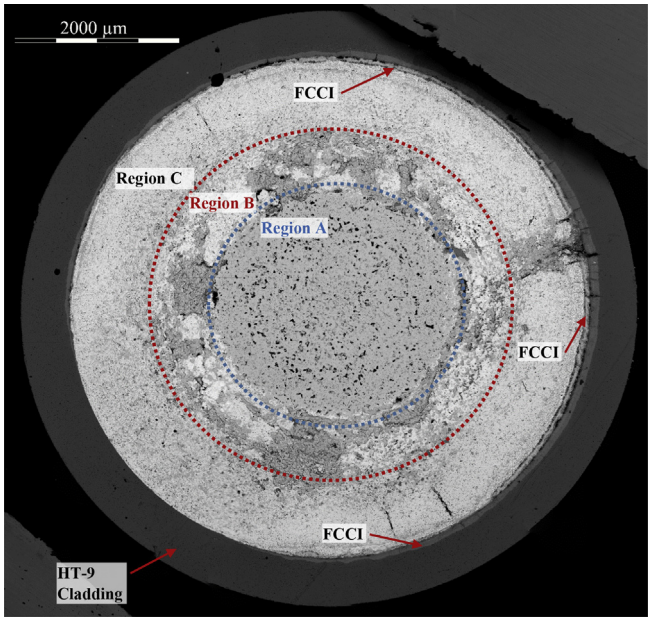

Fig. 1. Montage created from a set of BSE images showing the overall microstructure present in the cross section. The area inside the blue dotted line is referred to as the central region and the area between the blue and red dotted line is referred to as the middle region.

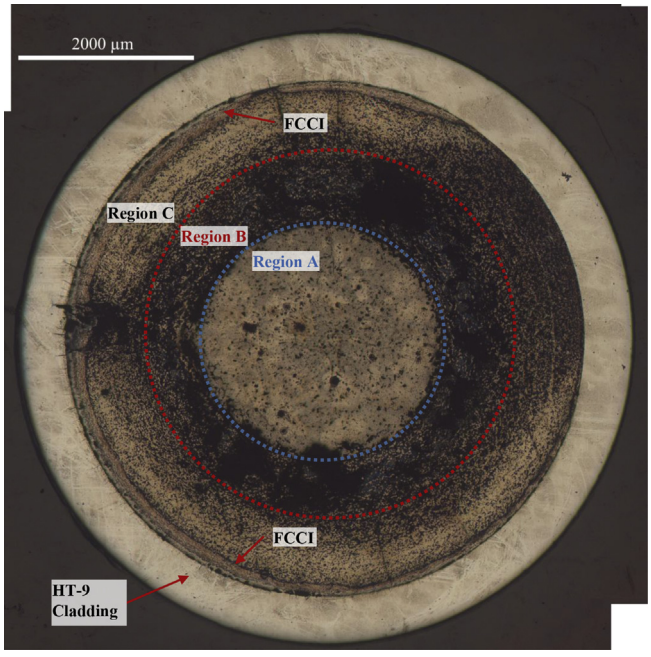

Fig. 2. Optical microscopy of MNT-83T.

layer that had formed on the cladding. The sample was decontaminated and coated with a thin layer of Au for conductivity.

Scanning electron microscopy exams were performed with a JEOL JSM-7000F field emission gun SEM equipped with WDS and EDS and Oxford INCA software. Images were collected using secondary electron (SE) and backscatter electron (BSE) detectors, and elemental analysis was performed with energy dispersive spectroscopy (EDS), and wavelength dispersive spectroscopy (WDS). The primary method for element identification in this work was EDS. In most cases there was clear elemental separation in the EDS spectrum and calibrated standards were not available for WDS quantitative analysis. Consequently there was little advantage to collecting data with WDS.

3. Results and discussion

3.1. Overall observations from the cross section

Initial SEM examinations of the cross section were focused on generating an overall image of the microstructure by BSE imaging. The BSE images allow grey-scale contrast to be seen between areas with different average atomic number (Z). The contrast illuminates compositional difference, the thrust of these examinations. A set of BSE images were stitched together to create the montage image seen in Fig. 1. Images were stitched together using commercially available software (Photoshop CC). Image alignment during the automatic stitching was restricted to translations only. Approximately 50 images were used to create Fig. 1. Specific regions of the fuel cross section are noted in the montage for discussion purposes. In Fig. 1, the regions are labeled A to C from the center of the fuel out toward the cladding.

For comparison between optical and electron microscopy techniques, a montage of optical microscopy of the same cross section is shown in Fig. 2. The regions marked in Figs. 1 and 2 are meant as general guides to illustrate the observed microstructure and should not be considered quantitative. Multiple regions appear in the cross section that correspond to different physical phenomena present in fast reactor metal fuel performance. For instance, the darker inner most region, Region A, in Fig. 1, indicates a lower average atomic number (Z) in this region. Region A would have been at irradiation temperatures above the γ phase transition temperature in U-10Zr (approximately 722 °C initially then lowering as more U is consumed by fission and Zr migrates into region A) [9,14]. Zirconium is more soluble in γ phase U and preferentially migrates to the γ phase regions. The added zirconium brings down the average Z of the U-Zr mixture. The porosity in this

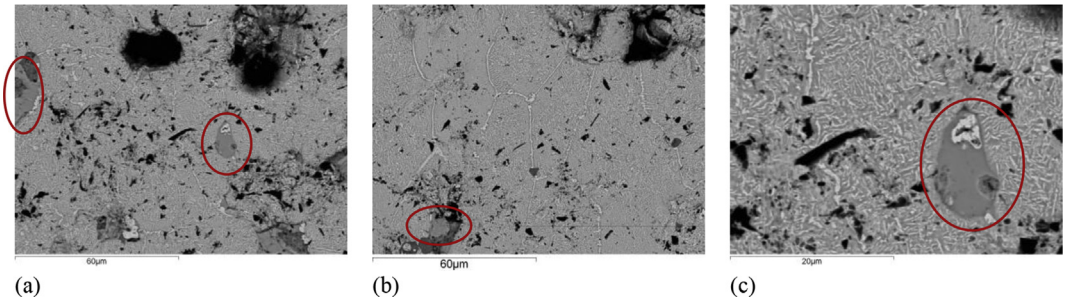

Fig. 3. Backscatter electron images of the region A of the fuel cross section (a) containing Pd-Ln precipitates, (b) an additional region with a precipitate, (c) a higher magnification image with Pd-Ln precipitates highlighted by red circles. (For interpretation of the references to colour in this figure legend, the reader is referred to the web version of this article.)

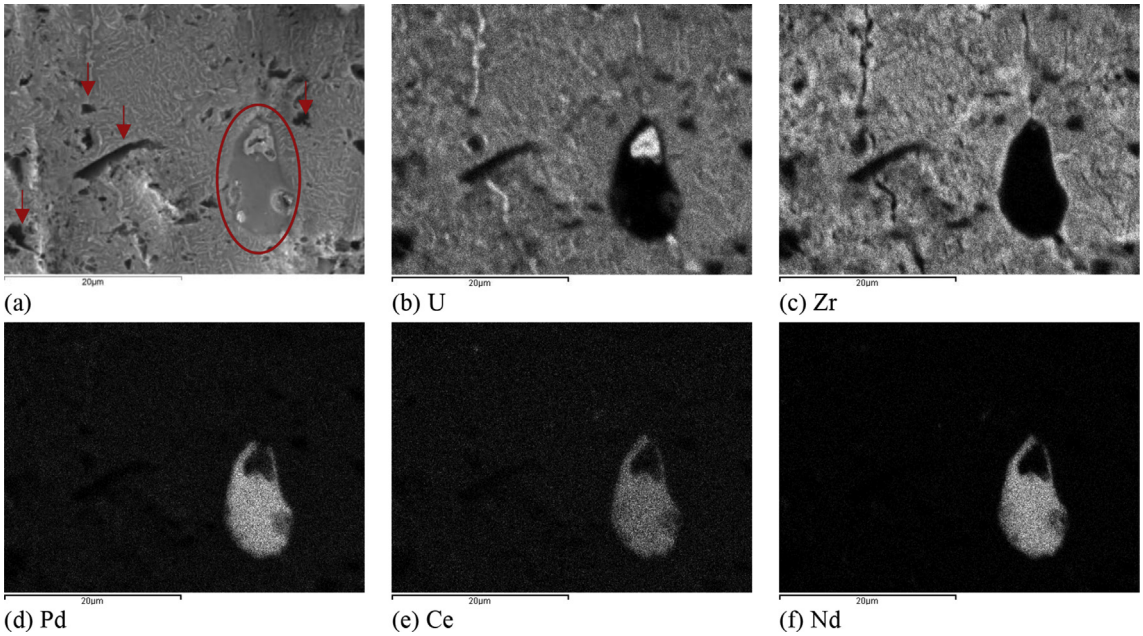

Fig. 4. (a) Secondary electron images of region A of the fuel cross section showing porosity (arrows) and a Pd-Ln precipitate (circle) and EDS maps of (b) U, (c) Zr, (d) Pd, (e)Ce, and (f) Nd.

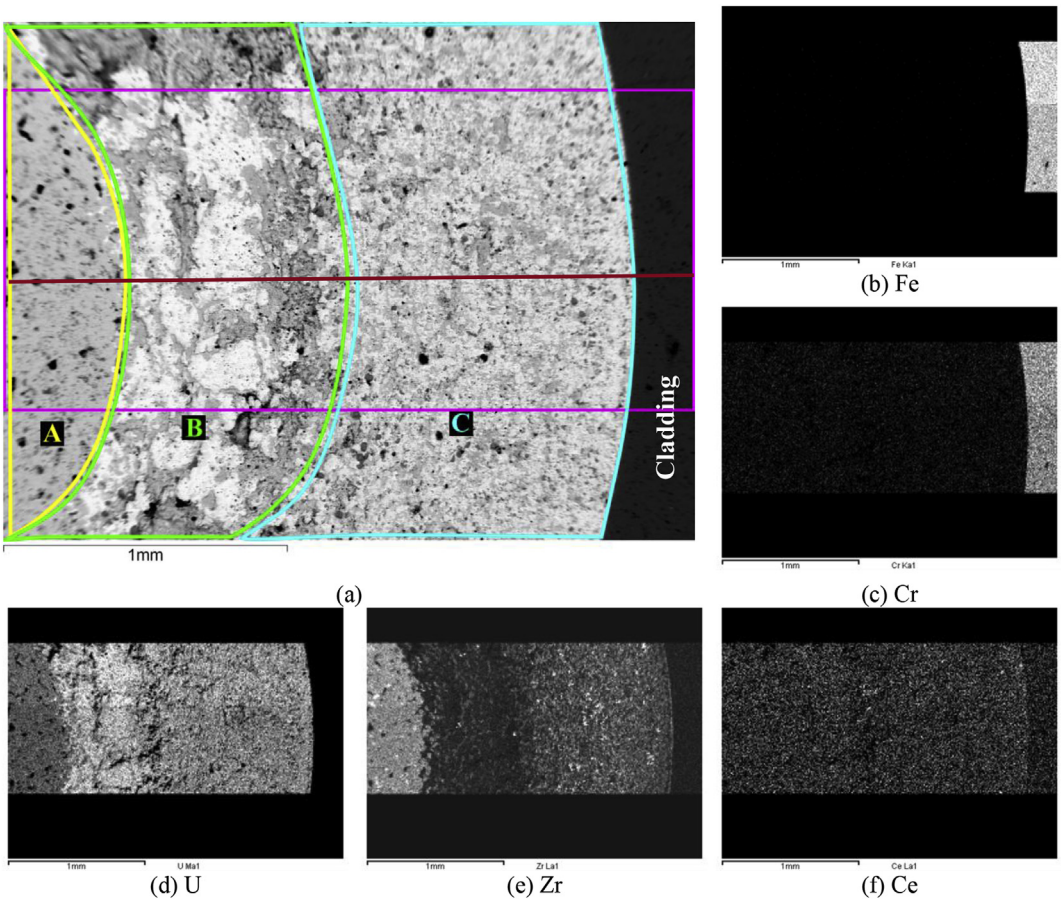

Fig. 5. EDS mapping of a radial sector of fuel without FCCI (a) BSE image of the mapped region, relative intensity of different x-ray peaks measured by EDS for (b) Fe $K_{\alpha 1}$, (c) Cr $K_{\alpha 1}$, (d) U $M_{\alpha 1}$, (e) Zr $K_{\alpha 1}$, (f) Ce $L_{\alpha 1}$.

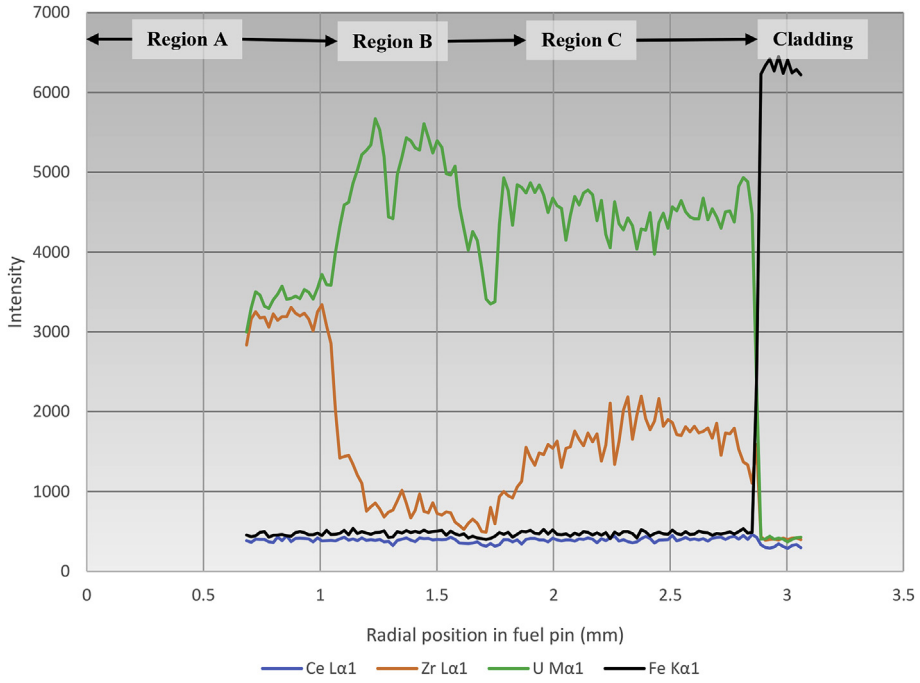

Fig. 6. EDS Line scan showing the relative intensity of x-ray peaks from U, Zr, Ce, and Fe across a radial fuel section without FCCI.

region is also largely spherical which also reflects the properties of the cubic γ phase of the high temperature solid solution (U, Zr). This behavior follows the historically observed microstructure [15].

Beyond Region A, the Zr content is depressed. In the areas where the sample is completely planar the Z contrast in Region B is brighter/lighter than in Region A or Region C. In Fig. 1 Region B has suffered some enhanced degradation due to oxidation. The loss of Zr to Region A makes the remaining high U content region more susceptible to oxidation. Approximately 5 years have passed between the original sample preparation and optical microscopy and the current SEM exam. This allowed for some significant oxidation to occur in spite of the low O_2 conditions of the storage inside the HFEF hot-cell. This oxidation is commonly observed in sample of metallic fuel that are stored for an extended period of time. Aggressive regrinding of the sample was undesirable in order to preserve the features of the FCCI layers that were observed in the original optical microscopy. The inability to fully remove the oxidation in Region B leads to the darker contrast seen in Fig. 1 in portions of Region B.

Region C between the cladding and Region B appears to have an overall U-Zr composition as evaluated by EDS near 10% Zr similar to the as-fabricated fuel. It operated in the alpha phase temperature regime of the U-Zr binary alloy (below 617 °C) [9]. It is more apparent at higher magnifications, but there is also evidence of phase separation between U and Zr in this fuel zone. This is expected in the alpha regime where there is little solubility for Zr in the U and delta phase (UZr_2) forms.

At the fuel cladding interface there are several distinct layers of FCCI. Each of these layers will be discussed in detail. In Fig. 1, it is worth noting the asymmetry of the FCCI. There is significant (>125 μm) cladding 'wastage' in the region of the pin shown in the upper right corner of Fig. 1, while there is no evidence of FCCI in the region of the cross section shown in the lower left corner of Fig. 1. The interaction zone is referred to as 'wastage' because the interaction layer is very brittle and often cracked, providing no strength to that layer of the cladding.

3.2. Central region (region A)

Higher magnification images of the central region are shown in Fig. 3. The typical microstructure of the region can be seen in Fig. 3 (a) and (b). Large area EDS scans of this region indicate that U-Zr mixture is between 70 and 65 wt % U and 30 to 35 wt% Zr. This region is above the γ phase transition temperature during irradiation, but after cooling the U and Zr have segregated into αU and δUZr_2 as predicted by the phase diagram. These two phases are shown stacked together throughout Fig. 3 as a white phase (αU) and a medium grey phase (UZr_2.).

In addition to the overall U-Zr mixture, there are several precipitates present.

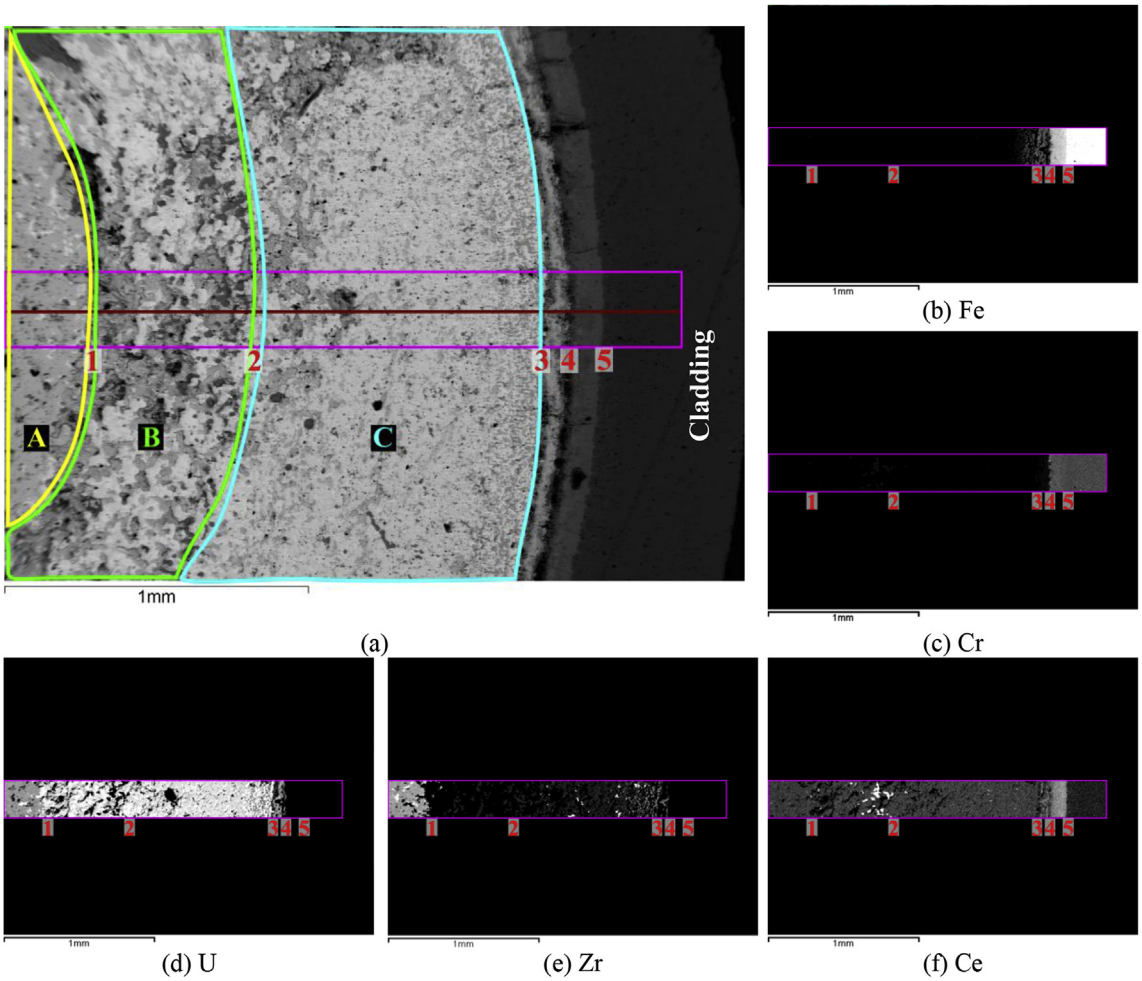

Fig. 7. EDS mapping of a radial sector of fuel with FCCI (a) BSE image of the mapped region, relative intensity of different x-ray peaks measured by EDS for (b) Fe $K_{\alpha 1}$, (c) Cr $K_{\alpha 1}$, (d) U $M_{\alpha 1}$, (e) Zr $K_{\alpha 1}$, (f) Ce $L_{\alpha 1}$.

Most notably the precipitate highlighted in Fig. 3(c) by the red circle contains a mixture of Pd and lanthanide (Ln) fission products. Analysis by EDS indicates this precipitate contains 27% Pd, 6% Y, 10% La, 15% Ce, and 41% Nd. This precipitate had a composition that is similar to several other precipitates located in the central region also highlighted by red circles in Fig. 3. The observation of these precipitates was predicted by Mariani [16–18] and was thought to have assisted in the relatively good FCCI performance of U-5wt.%Fs (Fs – fissium, a mixture of Mo, Ru, Rh, Pd, Zr and Nb) driver fuel utilized by EBR-II. This lead to the recent irradiation of U-10Zr with 1–4% Pd additives to mitigate FCCI [19,20]. The yield of the lanthanide fission products is much greater than the yield of Pd, so only some lanthanides are tied up in Pd-Ln intermetallics. Many free lanthanides are still available to migrate to the cladding and facilitate FCCI.

There are also some predominately Zr inclusions present in the central region. The SE image of the region shown in Fig. 3(c) is shown in Fig. 4(a) to better display the porosity in this region. Additionally, EDS mapping was performed over this region and is shown in Fig. 4 for U (b), Zr, (c), Pd, (d), Nd (e), and Ce (f). The lanthanide elements incorporated into these Pd-Ln precipitates in the central region of the fuel may indicate a sink for lanthanides that prevent migration of the lanthanides to the cladding where they form FCCI by interdiffusion with the cladding elements. The addition of Pd to U-Zr alloy fuel has been proposed as a technique to mitigate FCCI in U-Zr fuel [16–18]. The presence of these precipitates in this sample, especially in the high temperature areas, is evidence that this mitigation strategy may impede lanthanide migration. The exact phase of the Pd-Ln precipitate cannot definitively be determined from EDS exams alone. Future planned transmission electron microscopy (TEM) is planned on Focused Ion Beam (FIB) lift-outs from these precipitates. Electron diffraction should be able to identify the crystal structure of the precipitates. The observed precipitates contain much less Pd than used to capture simulated lanthanide carry-over in Mariani 2011 where 4 wt% Pd was used to immobilize lanthanides [16]. The Pd in the MFF fuel of this study is present only as a fission product, not an alloying element. The observed Ln-Pd ratio possibly indicates that a lower Pd content alloy (<4 wt%) of U, Pd and Zr may exist that can capture lanthanides created from fission and mitigate FCCI.

3.3. General microstructure of the fuel regions and zirconium redistribution

In the identified FCCI regions in Figs. 1 and 2, the cross-section microstructure of the FCCI is not uniform, which allows for the study of radial sectors that contain FCCI layers and comparison with those that do not contain FCCI layers. The portions not effected by FCCI offer a good opportunity to collect data on the constituent redistribution of Zr in the fuel. This phenomenon is well known in U-10Zr fuel from EBR-II experience but elemental measurements of this phenomenon are limited to a few historic EPMA exams [9,21,22]. The existence of redistribution of Zr in fuel pins is also limited to axial portions of pins that were operated with a significant radial portion of the fuel above the γ phase transition temperature for the alloy. This limited data set and interpretation of optical microscopy has become the basis for current modeling efforts of both the U-10Zr and the ternary U-Pu-10Zr system [23]. This exam provides a new set of data for U-10Zr irradiated in FFTF conditions. This data will be available for testing new constituent redistribution models. This is complementary to other work that has been performed on U-Pu-10Zr irradiations [24].

A radial sector of irradiated fuel without FCCI layers is shown in Fig. 5 along with EDS mapping of the highlighted region on the BSE image (a). The Fe (b) and Cr (c) appear to have not interacted with the fuel in any significant manner. The redistribution of the fuel can

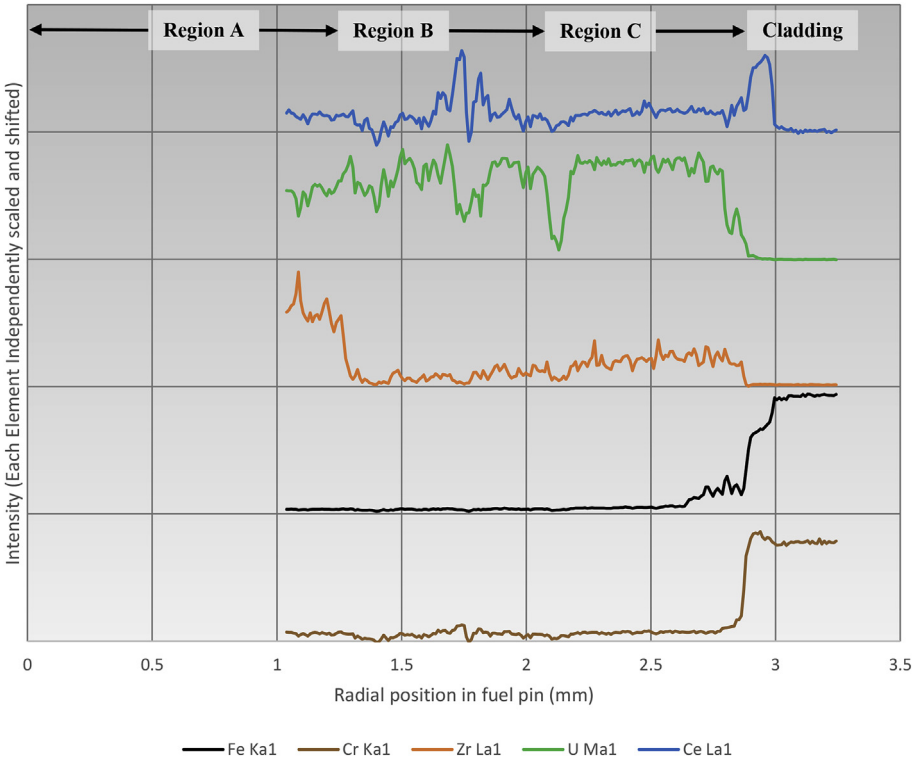

Fig. 8. EDS line scan showing the relative intensity of x-ray peaks from U, Zr, Ce, and Fe across a radial fuel section with FCCI. Each element has been independently scaled and shifted to show relative intensity changes across the fuel radius.

be clearly seen in the contrast of the BSE image (a) and by comparing the U and Zr EDS maps (d) vs (e). There were no areas where Ce or other lanthanide fission products concentrated into precipitates in this mapping area as illustrated by the Ce map in Fig. 5(f). The Zr redistribution results in 3 major fuel zones highlighted by A, B, and C in Fig. 5(a). Region A represents where the fuel was likely above the γ phase transition temperature where Zr in more soluble leading to the migration of Zr into this region. EDS evaluations of the average Zr concentration in Region A show that the Zr concentration is about 33 wt %. Region B is depleted in Zr caused by the migration of Zr to Region A. This region has only about 4 wt % Zr. It should also be noted that the darker parts of this region are primarily due to imperfections in the preparation of the sample. This region of the sample is more perceptible to oxidation and pullout during preparation due to its low Zr concentration. Region C retains the as-fabricated Zr concentration of about 10 wt% on average, but there is some U-Zr phase separation locally.

The results of the mapped region were converted to a radial line scan by collecting the results of the mapped region 20 μm to either side of the maroon line in Fig. 5(a). The x-ray peak intensities for U, Zr, Ce and Fe are plotted against pin radius in Fig. 6. Dips in uranium intensity in Fig. 6 at 1.3 and 1.7 mm are likely due to surface defects in Region B and not a true reduction in U content. The intensities in Fig. 6 are not corrected for background. Any small Fe signal in the fuel (below an intensity of 600) is likely background, and the U, Zr, and any small Ce signal in the cladding (f) is due to interference with the Cr $K_{\alpha 1}$ line.

3.4. Radii with FCCI

Three low magnification radial sector EDS scans were collected in regions where the FCCI was present. The extra FCCI layers complicate the interpretation of the EDS data, and their microstructural characteristics are discussed in detail in the next section. At the whole radius scale, the behavior of Fe, Cr, U, Zr, Ce, and other elements were recorded by EDS mapping. The maps were then converted to a line scan down the center of the mapped area that captured the average response of the mapping. In these maps, data is collected from the same Zr redistribution regions as were highlighted in Fig. 5(a) through to the FCCI layers and into the cladding. The same regions (A, B, C) defined in Figs. 1 and 5(a) are used in Fig. 7(a) up to the first FCCI radial sector. EDS maps of Fe, Cr, U, Zr, and Ce are shown in Fig. 7(b) through Fig. 7(f) respectively. Additionally 5 marks (labeled 1–5) have been added to all the images in Fig. 7 to show positional relationships between the images. The migration of Zr in relation to U can be observed by comparing Fig. 7(d) and (e). The outer radius of region C in Fig. 7 is different that the sector without FCCI.

A greater amount of phase separation between U and Zr can be observed in radial sectors with FCCI. This corresponds to Fe

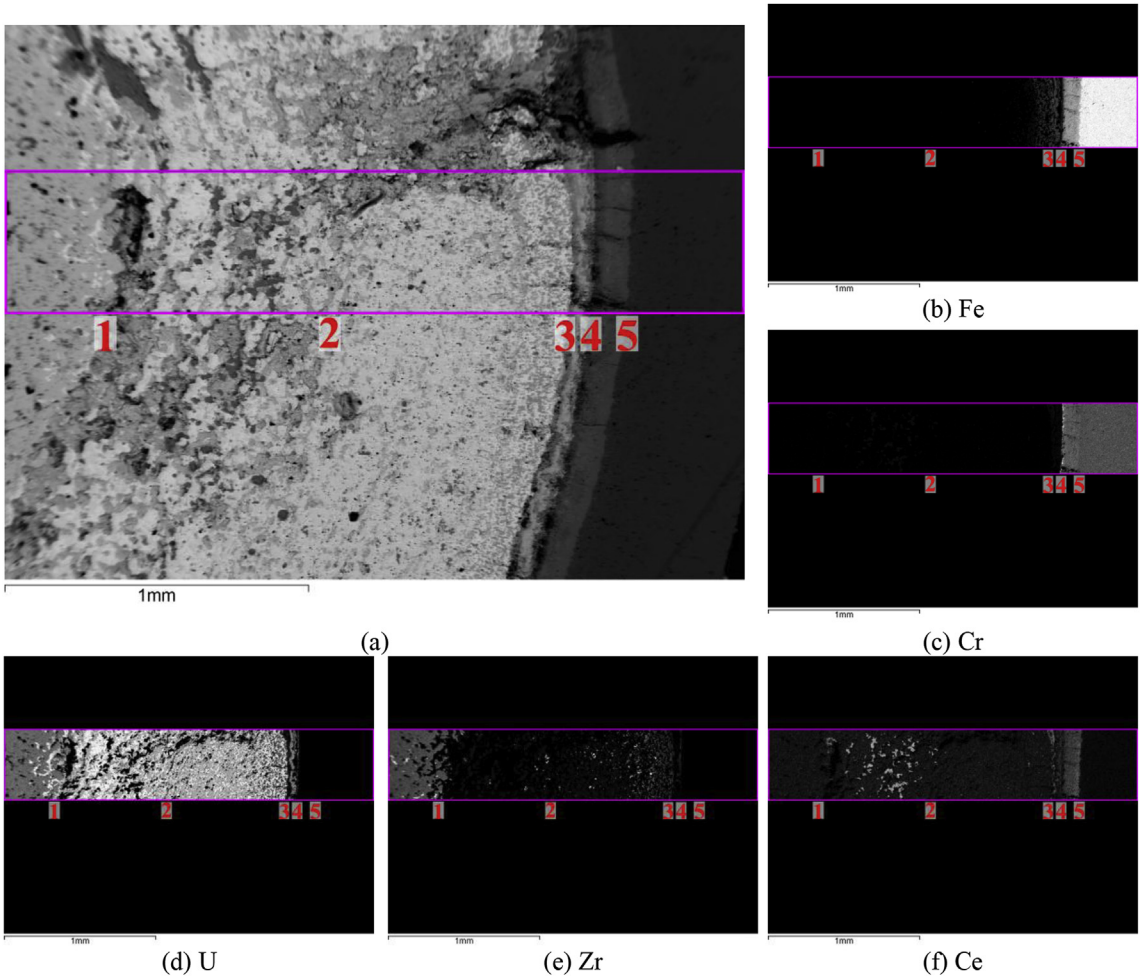

Fig. 9. EDS mapping of a radial sector of fuel with FCCI (a) BSE image of the mapped region, relative intensity of different x-ray peaks measured by EDS for (b) Fe $K_{\alpha 1}$, (c) Cr $K_{\alpha 1}$, (d) U $M_{\alpha 1}$, (e) Zr $K_{\alpha 1}$, (f) Ce $L_{\alpha 1}$.

infiltration into this part of the fuel. This is different from the more discreet layers closer to the cladding. The first light grey layer beyond Region C is a mixture of U, Fe, and lanthanides. The next darker grey layer is a mixture of Fe, Cr and lanthanides. The boundary between the lighter and darker grey layers in Fig. 7(a) is likely the original boundary between the cladding and the fuel as Cr is present in the darker grey layer, but not the light grey layer. The Cr signal rises slightly in the darker layer because of the migration of Fe into the fuel. In addition to concentrating near the cladding, precipitates of lanthanide fission products are found near mid radius in region B of the fuel.

The radial distribution of different elements along the maroon EDS line scan in Fig. 7(a) are shown in Fig. 8. In this EDS line scan, the different regions can more easily be ascribed to radial locations. The in-pile gamma phase ends at a radius of about 1.25 mm from fuel pin centerline as indicated by the abrupt drop in Zr signal. The drop in U signal from 2.1 to 2.2 mm is due to porosity or a polishing defect in the sample. From 2.2 to 2.8 mm the U and Zr ratio is roughly representative of U-10Zr. The area from 2.8 to 2.85 mm is the mixture of Ce with the U and iron represented by the light grey layer. Iron starts to migrate into the U and Zr causing phase separation at about 2.6 mm, and the Fe-Ce (lanthanide) layer represented by dark grey in the BSE image is between 2.85 and 3.0 mm. Beyond 3.0 mm the cladding appears representative of HT-9 at this scale. However, at higher magnifications it was shown that lanthanide attack continues locally along preferential pathways. This is discussed in the FCCI Layers section.

A similar set of EDS maps and line scans are included for two additional radial sectors. Fig. 9 and Fig. 10 for the second sector and Fig. 11, and Fig. 12 for the third sector. As with Fig. 7, there is a set of numbered marks in Figs. 9 and 11 to show positional relationships between the images. In the second sector, which is located just below a large crack in the fuel, the same behavior as the first radial sector is largely observed in Fig. 9. An EDS line scan for Nd has been added to Fig. 10 to highlight some of the differences in behavior that can be seen between the Nd and Ce lanthanides. In Fig. 11(c), there is some peak overlap between Cr x-rays and lanthanide x-rays that creates a region of low intensity in the interior of the fuel.

3.5. FCCI layers

The FCCI layers formed in U-10Zr fuel irradiated in EBR-II were studied by Keiser [8]. Specifically Keiser studied fuel pins from EBR-II experimental assemblies. The fabrication of the MFF3 fuel is largely the same as the EBR-II fuel; the fuel slugs were cast using the same fabrication processes and equipment. The layers observed in this work appear to be slightly more complex than those observed by Keiser. In this cross section, approximately three quarters of the observed HT-9 circumference exhibits some degree of FCCI. The layers of the FCCI are well illustrated in Fig. 13. EDS mapping of the region shown in Fig. 13 is shown in Fig. 14. The key elements in the different layers are represented in Fig. 14 including Cr, Fe, U, Zr, Ce and Nd. These figures demonstrate the complexity of the FCCI layers described in this paragraph. These FCCI layers were observed throughout the fuel cladding interface in this sample.

The layers (A to F) will be generally described followed by more semi-quantitative results from EDS analysis of each layer. On the left side of the figure is intact HT-9 cladding (Layer A) where there are little to no lanthanide fission products observed. Further towards the fuel/cladding interface is a layer of HT-9 (Layer B) that

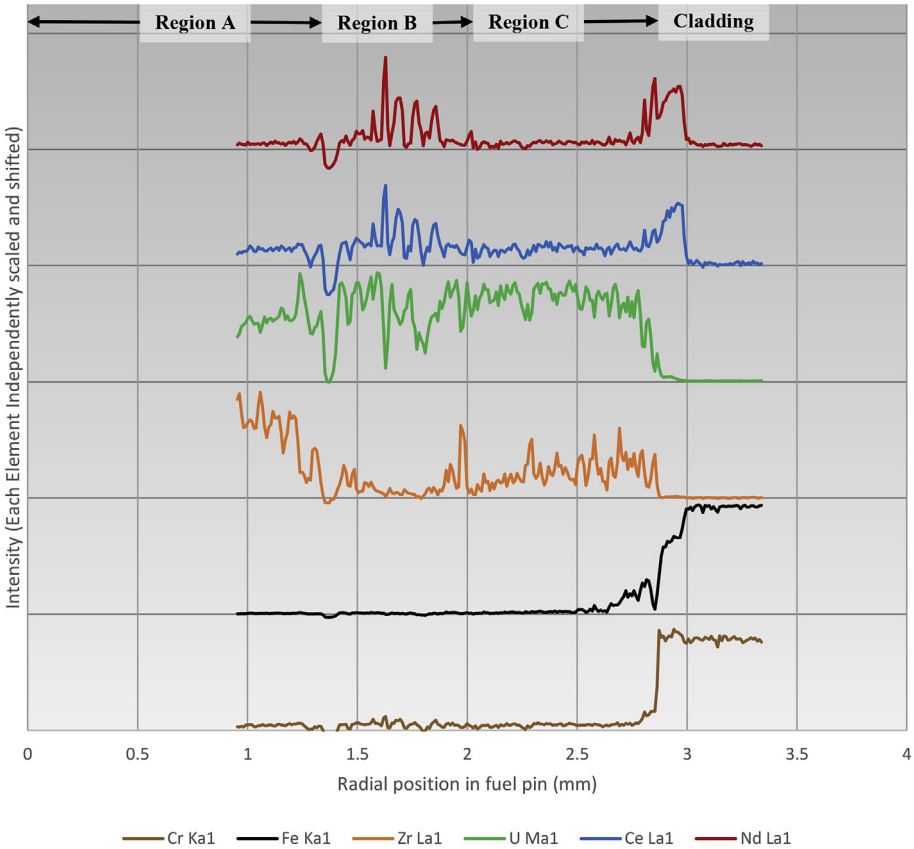

Fig. 10. EDS line scan showing the relative intensity of x-ray peaks from Cr, Fe, Zr, U, Ce, and Nd across a radial fuel section with FCCI. Each element has been independently scaled and shifted to show relative intensity changes across the fuel radius.

has been infiltrated by lanthanides along the prior-austenite grain boundaries. This zone is not observable in optical microscopy and has likely not been well characterized in historical PIE of metallic fast reactor fuel. The degree to which this layer has a deleterious effect on the cladding is not currently understood. Whether or not this layer can be related to the denuded zone [25] observed by etching HT-9 cladding followed by optical microscopy needs to be further investigated.

The next layer (Layer C) is dark grey in Fig. 13 and is a mixture of HT-9 components and lanthanide fission products. The density of Cr in this layer appears to be unchanged from the density of Cr in HT-9. The amount of Fe in this layer is depleted compared to the bulk cladding by iron migrating into the fuel. A significant amount of lanthanides migrate into the cladding material in this layer. Inagaki and Ogata have determined using diffusion couples that this layer looks to be $(Fe,Cr)_{17}Ln_2$ or a mixture of $(Fe,Cr)_{17}Ln_2$ and $(Fe,Cr)_3Ln$ [26]. Elemental identification of this area by EDS in the current study finds this region to be 74% Fe, 15% Cr, 4% Ce, and 7% Nd, in weight percent.

The next layer (Layer D) towards the center of the fuel is made primarily of U, Fe and lanthanides. This layer contains no Cr. The entire region was measured to be about 60% U, 28% Fe, 6%La and 6% Nd (all weight percent) by EDS. The EDS maps in Fig. 14 reveal bands of U-Fe and Ln-Zr mixtures in this layer. The next layer (Layer E) contains clear phase segregation. The light phase is a mixture of U and Fe. The grey phase is a mixture of Zr and Fe. This layer also contains lanthanide precipitates with Y and Sr as dark grey phases in Fig. 13. Further into the fuel (Layer F), the microstructure is representative of a binary solid solution of U and Zr similar to the as-fabricated structure with only occasional fission product precipitates. This region is 89 wt % U and 11 wt % Zr by EDS.

The multiple FCCI layers were examined in further detail in Fig. 15. Point scans were taken at several different locations in this region. The results of these scans are summarized in Table 1. Point scans 1 and 12 both appear to have the major elemental composition of HT-9 with approximately 12% Cr and 88% Fe. This indicates that although there is some lanthanide infiltration into this area, the lanthanide infiltration is along discrete pathways such as the prior-austenitic grain boundaries. Points 2 and 11 have similar compositions, where some of the Fe appears to have been replaced with Ce and Nd. Points 3 and 10 have the same compositions at the limits of EDS characterization of 30% Fe and 70%U. This composition is very close to UFe_2 although additional exams would need to confirm if this is the actual compound. Both of these points are free from lanthanides, but there are bands of lanthanides in the layer as shown in Fig. 14. Points 5 and 9 have similar composition that is close to the expected composition of U_6Fe. Phase diagrams for the complex system that exists in FCCI layers do not exist, but insight into the likely compounds that are forming can be inferred from binary and ternary equilibrium phase diagrams [8]. Both UFe_2 and U_6Fe exist on the binary U-Fe phase diagram, so it is likely that these compounds can form in the interaction zones. The remaining

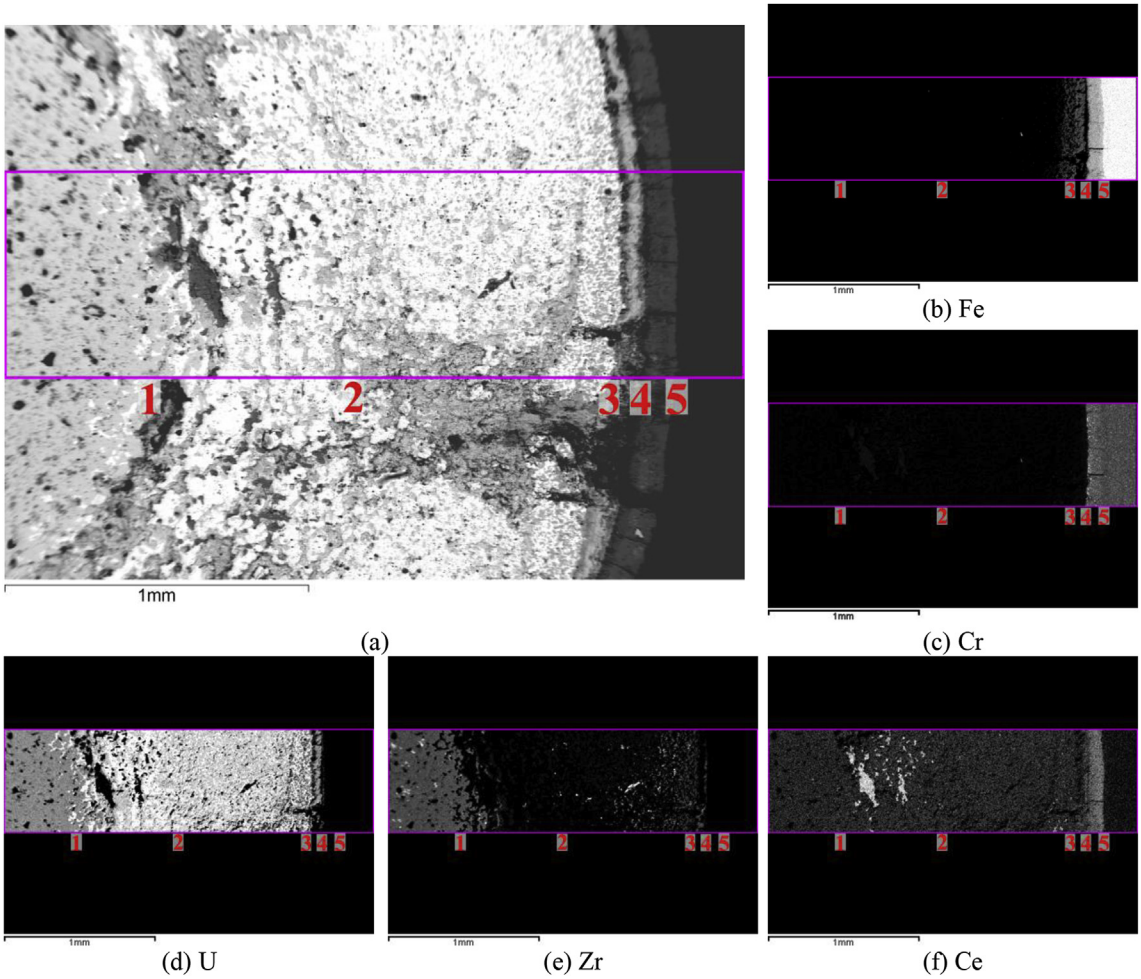

Fig. 11. EDS mapping of a radial sector of fuel with FCCI (a) BSE image of the mapped region, relative intensity of different x-ray peaks measured by EDS for (b) Fe $K_{\alpha 1}$, (c) Cr $K_{\alpha 1}$, (d) U $M_{\alpha 1}$, (e) Zr $K_{\alpha 1}$, (f) Ce $L_{\alpha 1}$.

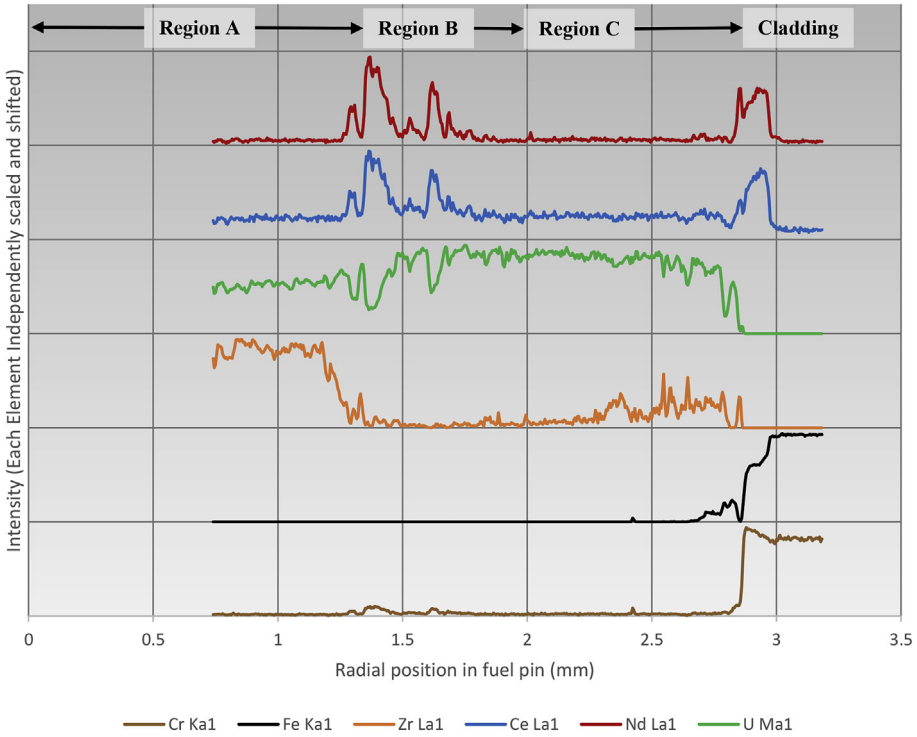

Fig. 12. EDS line scan showing the relative intensity of x-ray peaks from Cr, Fe, Zr, U, Ce, and Nd across a radial fuel section with FCCI. Each element has been independently scaled and shifted to show relative intensity changes across the fuel radius.

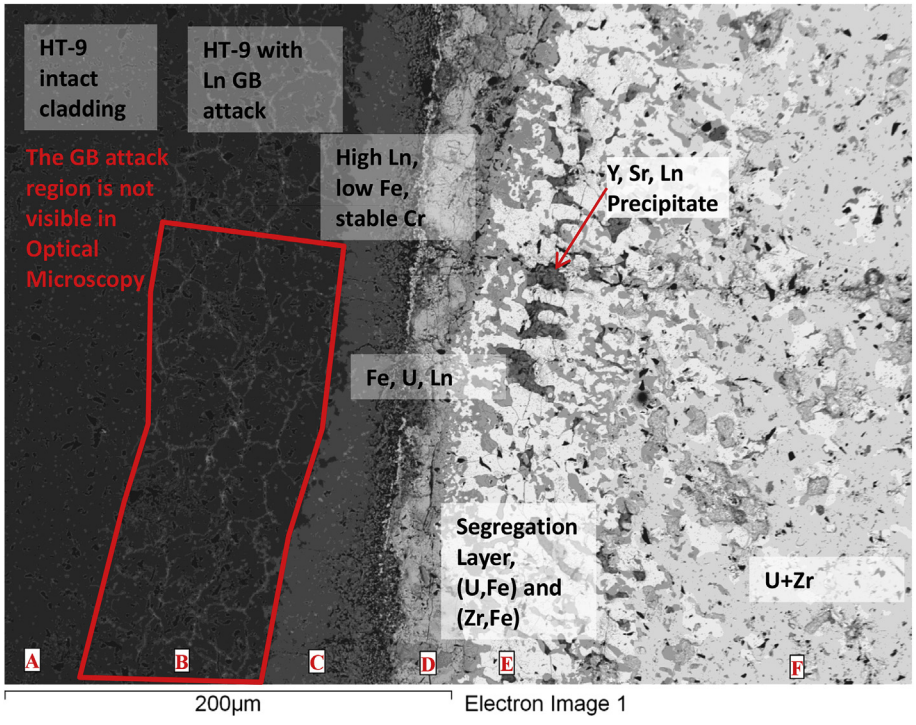

Fig. 13. Generally observed FCCI layers in the sample with labels describing each layer (Ln = Lanthanides, GB = Grain Boundary).

EDS spot measurements are all somewhat distinct. Points 4, 8 and 13 all appear to be similar in the BSE image, but each has a unique composition. Points 6 and 7 are located in lanthanide precipitates. However the precipitate at Point 6 contains Y and Sr while the precipitate at Point 7 does not. Both Y and Sr tend to be miscible with lanthanides. The presence of these fission products with the Ln fission products is not surprising. Additional microcopy on these precipitates is necessary to further understand the observed phases.

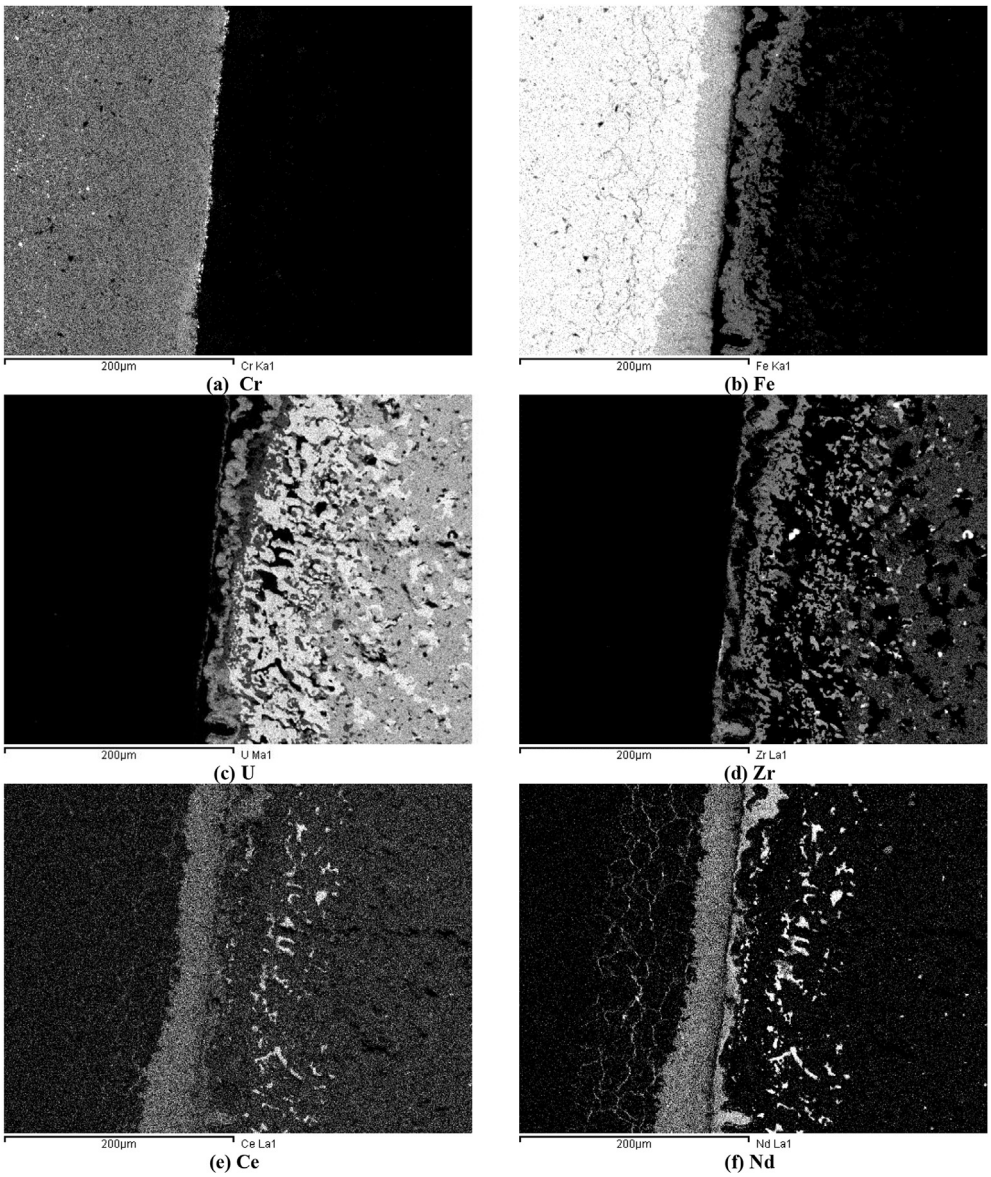

Fig. 14. EDS mapping of the FCCI layers shown in Fig. 13 (a) Cr $K_{\alpha 1}$ (b) Fe $K_{\alpha 1}$, (c) Cr $K_{\alpha 1}$, (d) U $M_{\alpha 1}$, (e) Ce $L_{\alpha 1}$, (f) Nd $L_{\alpha 1}$.

3.6. HT-9 precipitates

The mid-thickness of the HT-9 cladding was examined and found to contain many Mo and W rich precipitates. The HT-9 cladding has a nominal composition of Fe-12Cr-0.2C-0.25Si-0.2Mn-0.5W-0.5 V-1Mo-0.5Ni where the number preceding the element is the weight percent and Fe is the balance of the composition [13]. A typical BSE image of the cladding mid-thickness from this sample is shown in Fig. 16. The image shows the Mo-W rich precipitates (light grey) in HT-9 cladding (dark grey). The black areas that appear to be porosity are unexpected. It is likely damage from sample preparation (pull-out). In the precipitates, the major elements present in higher amounts than in the bulk are Mo and W. In these precipitates EDS analysis indicates a Mo wt.% of about 14% and a W wt.% of about 6%. The Cr content appears to be the same as the bulk and the Fe concentration is reduced. The relative amount of C signal from these precipitates is higher than the bulk material. The identified Mo-W rich phase is not present in unirradiated HT-9 and is likely a result of irradiation-enhanced thermal precipitations. The modest dose (50–60 dpa) and high operating temperature of this cladding (615 °C) are not unique amongst test parameters for HT-9, but most materials test examinations focused upon void formation and not the nature of precipitates. It is theorized that the Mo-W precipitates are likely Chi or laves phase [26,27]. Further examination of this cladding by transmission electron microscopy (TEM) is planned and will help to clarify the phase of the Mo-W precipitates. More important than the exact nature of the phase is that the existence of the thermal and/or radiation induced phase has implications for cladding performance by reducing cladding ductility.

4. Conclusions

Many different macroscopic and microscopic fuel performance phenomena were observed in the examination of this cross section from HT-9 clad, U-10Zr MFF3 pin #193045 at x/L = 0.98. SEM observations were focused on evaluating constituent redistribution and evaluating the morphology of the fuel/cladding chemical

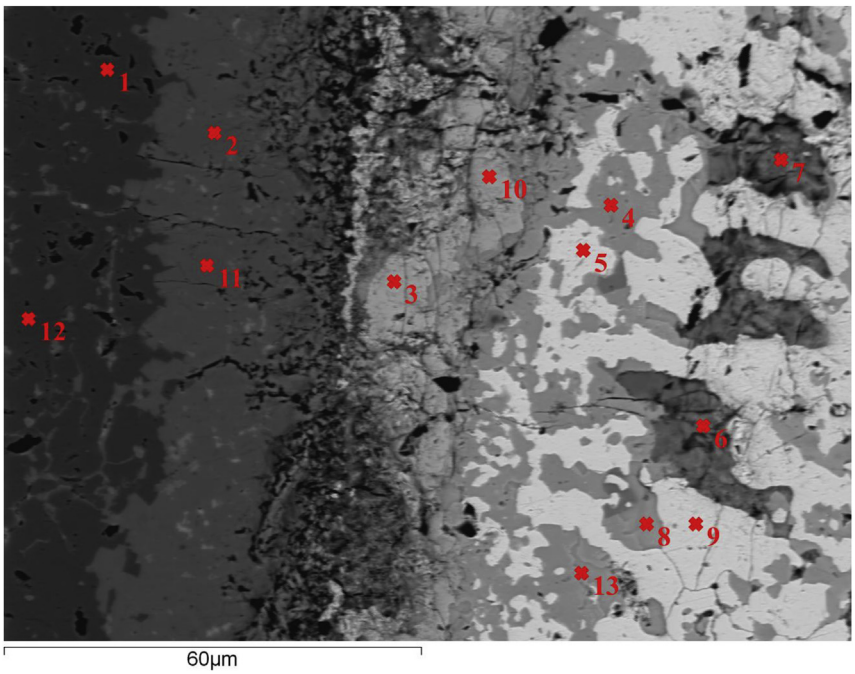

Fig. 15. FCCI interaction layers from Fig. 13 at a higher magnification showing EDS spot measurement locations.

Table 1
Results from EDS scan of different phases in the FCCI region.

Spectrum	Elemental composition (wt.%)	Spectrum	Elemental composition
1	12% Cr, 88% Fe	8	7% Fe, 18% Pd, 11% La, 10% Ce, 32% Nd, 6% Sm, 15% U
2	13% Cr, 74% Fe, 5% Ce, 8% Nd	9	4% Fe, 96% U
3	30% Fe, 70% U	10	30% Fe, 70% U
4	24% Fe, 45% U, 31% Zr	11	14% Cr, 74% Fe, 5% Ce, 7% Nd
5	4% Fe, 96% U	12	13% Cr, 87% Fe
6	7% Sr, 47% Y, 4% La, 5% Ce, 4% Pr, 25% Nd, 8% Sm	13	19% Fe, 25% Zr, 5% Pd, 7% Nd, 44% U
7	20% La, 24% Ce, 13% Pr, 38% Nd, 5% Sm		

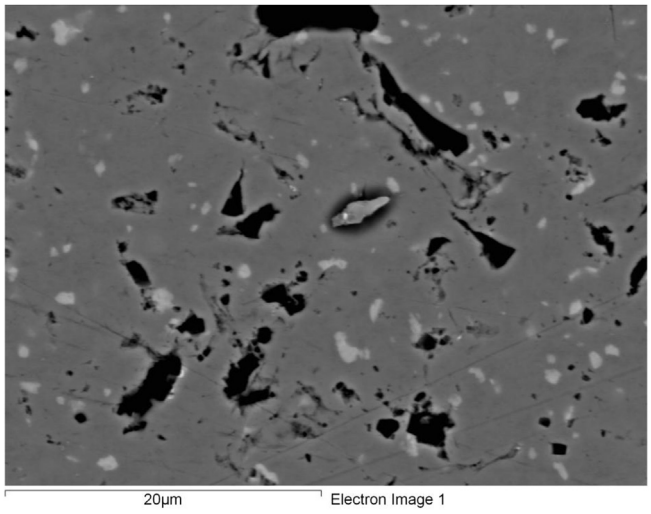

Fig. 16. Typical mid-thickness cladding BSE image showing the Mo-W rich precipitates (light grey) in HT-9 cladding (dark grey).

interaction (FCCI) layers. This portion of fuel (top of fuel column) was chosen because it operates at relatively high temperatures (FCCI and phase-related radial zone formation) while having a reduced burnup and therefore lower radiation field and easier to handle full cross-sections for detailed electron microscopic examinations.

Clear Zr redistribution occurred resulting in a much higher Zr content in the center of the fuel. Several line scans have been completed in an effort to better understand constituent redistribution at this local burnup and temperature condition. The observation of precipitates of Pd and lanthanides in the central region is notable and supports the continued development of metal fuel additives that can mitigate FCCI at high burnup. Mo-W precipitates were observed in the cladding, which are novel and likely produced by a combination of the high temperature and modest dose conditions in the fuel.

On a finer scale the FCCI layers were examined. The morphology of the FCCI layers is complex. Lanthanide fission products are transporting to the cladding interface, attacking the cladding and Fe from the cladding is entering the fuel. The Fe entering the fuel appears to be causing some phase segregation between the U and Zr near the cladding. An intergranular infiltration of lanthanide fission products into the cladding is of special interest because this phenomenon cannot be observed readily with optical microscopy and may represent a weaker layer in the cladding that has not been fully considered in previous fuel performance studies. The FCCI layers will be studied in greater detail at smaller length scales utilizing Transmission Electron Microscopy and sample preparation

by Focused Ion Beam. Examination of portions of the FCCI layers by synchrotron light source techniques would also be beneficial.

Disclosure statement

This manuscript has been authored by Battelle Energy Alliance, LLC under Contract No. DE-AC07-05ID14517 with the U.S. Department of Energy. The United States Government retains and the publisher, by accepting the article for publication, acknowledges that the United States Government retains a nonexclusive, royalty-free, paid-up, irrevocable, world-wide license to publish or reproduce the published form of this manuscript, or allow others to do so, for United States Government purposes.

Role of funding source

The funding source had no role in the research or writing of this paper, or the decision to submit it for publication.

Acknowledgements

This work was supported by the U.S. Department of Energy, Advanced Fuels Campaign of the Fuel Cycle R&D program in the Office of Nuclear Energy.

References

[1] G.L. Hofman, L.C. Walters, T.H. Bauer, The technology of the integral fast reactor and its associated fuel cycle metallic fast reactor fuels, Prog. Nucl. Energy. ISSN: 0149-1970 31 (1) (1997) 83–110, http://dx.doi.org/10.1016/0149-1970(96)00005-4.

[2] A.L. Pitner, R.B. Baker, Metal fuel test program in the FFTF, J. Nucl. Mater. ISSN: 0022-3115 204 (1993) 124–130, http://dx.doi.org/10.1016/0022-3115(93)90208-G.

[3] W.J. Carmack, H.M. Chichester, D.L. Porter, D.W. Wootan, Metallography and fuel cladding chemical interaction in fast flux test facility irradiated metallic U-10Zr MFF-3 and MFF-5 fuel pins, J. Nucl. Mater. ISSN: 0022-3115 473 (May 2016) 167–177, http://dx.doi.org/10.1016/j.jnucmat.2016.02.019.

[4] W.J. Carmack, D.L. Porter, D.G. Cummings, H.J.M. Chichester, S.L. Hayes, D.W. Wootan, Examination of Legacy Metallic Fuel Pins (U-10Zr) Tested in FFTF, INL/LTD-13–28987 r1, Idaho National Laboratory, 2013.

[5] J. Gan, D.D. Keiser Jr., D.M. Wachs, A.B. Robinson, B.D. Miller, T.R. Allen, Transmission electron microscopy characterization of irradiated U-7Mo/Al-Si dispersion fuel, J. Nucl. Mater. 396 (2010) 234–239, http://dx.doi.org/10.1016/j.jnucmat.2009.11.015.

[6] D.D. Keiser Jr., A.B. Robinson, J.-F. Jue, P. Medvedev, D.M. Wachs, M.R. Finlay, Microstructural development in irradiated U-7Mo/6061 Al alloy matrix dispersion fuel, J. Nucl. Mater. 393 (2009) 311–320, http://dx.doi.org/10.1016/j.jnucmat.2009.06.018.

[7] M. Teague, B. Gorman, B. Miller, J. King, EBSD and TEM characterization of high burn-up mixed oxide fuel, J. Nucl. Mater. 444 (2014) 475–480, http://dx.doi.org/10.1016/j.jnucmat.2013.10.037.

[8] D.D. Keiser Jr., 3.15-Metal fuel-cladding interaction, in: Rudy J.M. Konings (Ed.), Comprehensive Nuclear Materials, Elsevier, Oxford, 2012, ISBN 9780080560335, pp. 423–441, http://dx.doi.org/10.1016/B978-0-08-056033-5.00067-7.

[9] G.,L. Hofman, S.L. Hayes, M.C. Petri, Temperature gradient driven constituent redistribution in U-Zr alloys, J. Nucl. Mater. 227 (1996) 277–286, http://dx.doi.org/10.1016/0022-3115(95)00129-8.

[10] Y.S. Kim, G.L. Hofman, S.L. Hayes, Y.H. Sohn, Constituent redistribution in U-Pu-Zr fuel during irradiation, J. Nucl. Mater. 327 (2004) 27–36, http://dx.doi.org/10.1016/j.jnucmat.2004.01.012.

[11] D.D. Keiser Jr., Recent progress in metal fuel–cladding interaction research, in: Reference Module in Materials Science and Materials Engineering, Elsevier, 2016, ISBN 9780128035818, http://dx.doi.org/10.1016/B978-0-12-803581-8.00708-6. Current as of 28 October 2015.

[12] D.D. Keiser Jr., A.A.A.P. Olsson (Eds.), Nuclear Reactors, Nuclear Fusion, and Fusion Engineering, Nova Science, Hauppauge, NY, 2009.

[13] L. Leibowitz, R.A. Blomquist, Thermal conductivity and thermal expansion of stainless steels D9 and HT9, Int. J. Thermophys. 9 (5) (1988) 873–883, http://dx.doi.org/10.1007/BF00503252.

[14] Toru Ogawa, Takashi Iwai, Thermochemical modelling of U-Zr alloys, J. Less Common Metals. ISSN: 0022-5088 170 (1) (1991) 101–108, http://dx.doi.org/10.1016/0022-5088(91)90055-9.

[15] G.L. Hofman, R.G. Pahl, C.E. Lahm, D.L. Porter, Swelling behavior of U-Pu-Zr fuel, Metallurgical Mater. Trans. A 21 (2) (1990) 517–528, http://dx.doi.org/10.1007/BF02671924.

[16] R.D. Mariani, D.L. Porter, T.P. O'Holleran, S.L. Hayes, J.R. Kennedy, Lanthanides in metallic nuclear fuels: their behavior and methods for their control, J. Nucl. Mater. ISSN: 0022-3115 419 (1–3) (December 2011) 263–271, http://dx.doi.org/10.1016/j.jnucmat.2011.08.036.

[17] G.W. Egeland, R.D. Mariani, T. Hartmann, D.L. Porter, S.L. Hayes, J.R. Kennedy, Reducing fuel-cladding chemical interaction: the effect of palladium on the reactivity of neodymium on iron in diffusion couples, J. Nucl. Mater. ISSN: 0022-3115 432 (1–3) (January 2013) 539–544, http://dx.doi.org/10.1016/j.jnucmat.2012.07.028.

[18] G.W. Egeland, R.D. Mariani, T. Hartmann, D.L. Porter, S.L. Hayes, J.R. Kennedy, Reduction of FCCI effects in lanthanide–iron diffusion couples by doping with palladium, J. Nucl. Mater. ISSN: 0022-3115 440 (1–3) (September 2013) 178–192, http://dx.doi.org/10.1016/j.jnucmat.2013.04.060.

[19] H.J.M. Chichester, et al., Advanced metallic fuel for ultra-high burnup: irradiation tests in ATR, Trans. Am. Nucl. Soc. 106 (2012).

[20] J.M. Harp, H.J.M. Chichester, Highlights from the postirradiation examination of AFC-3A and AFC-3B, Trans. Am. Nucl. Soc. 114 (2016).

[21] J.E. Sanecki, Results of Electron Microprobe Examination of Two Specimens Taken from IFR Fuel Element DP-81, Argonne National Laboratory, Intra-Laboratory Memo, October 1991.

[22] J.E. Sanecki, Results of Electron Microprobe Examination of Specimen from Fuel Pin DP-11 from X447A (A/G 437A8), Argonne National Laboratory, Intra-Laboratory Memo, January 1993.

[23] J. Galloway, C. Unal, N. Carlson, D. Porter, S. Hayes, Modeling constituent redistribution in U–Pu–Zr metallic fuel using the advanced fuel performance code BISON, Nucl. Eng. Des. ISSN: 0029-5493 286 (May 2015) 1–17, http://dx.doi.org/10.1016/j.nucengdes.2015.01.014.

[24] L. Capriotti, S. Brémier, K. Inagaki, P. Pöml, D. Papaioannou, H. Ohta, T. Ogata, V.V. Rondinella, Characterization of metallic fuel for minor actinides transmutation in fast reactor, Prog. Nucl. Energy, Available online 7 May 2016, ISSN 0149-1970, http://dx.doi.org/10.1016/j.pnucene.2016.04.004.

[25] A.B. Cohen, H. Tsai, L.A. Neimark, Fuel/cladding compatibility in U-19Pu-10Zr/HT9-clad fuel at elevated temperatures, J. Nucl. Mater. ISSN: 0022-3115 204 (1993) 244–251, http://dx.doi.org/10.1016/0022-3115(93)90223-L.

[26] K. Inagaki, and T. Ogata. "Reaction of Lanthanide Elements with Fe-Cr Alloy," Journal of Nuclear Materials 441 (2013) p.574–578. YIREN CHEN, IRRADIATION EFFECTS OF HT-9 MARTENSITIC STEEL, Nuclear Engineering and Technology, Volume 45, Issue 3, June 2013, Pages 311-322, ISSN 1738-5733, http://dx.doi.org/10.5516/NET.07.2013.706.

[27] O. Anderoglu, J. Van den Bosch, P. Hosemann, E. Stergar, B.H. Sencer, D. Bhattacharyya, R. Dickerson, P. Dickerson, M. Hartl, S.A. Maloy, Phase stability of an HT-9 duct irradiated in FFTF, J. Nucl. Mater. ISSN: 0022-3115 430 (1–3) (November 2012) 194–204, http://dx.doi.org/10.1016/j.jnucmat.2012.06.038.